ISSN 0036-0244, Russian Journal of Physical Chemistry A, 2022, Vol. 96, No. 13, pp. 3038–3044. © Pleiades Publishing, Ltd., 2022.

PHOTOCHEMISTRY AND MAGNETOCHEMISTRY

Flower-Like $SrTiO_3/BiVO_4$ Heterojunction Nanocomposite Photocatalyst for Effective Degradation of Tetracycline

Xinglan Xiao[a,b], Yingna Zhao[a,b,*], Tao Liu[a,b], Jianchao Zhang[a,b], and Jiansheng Wang[a,b]

[a] *College of Material Science and Engineering, North China University of Science and Technology, Hebei, Tangshan, 063210 China*

[b] *Hebei Province Laboratory of Inorganic Nonmetallic Materials, Hebei, Tangshan, 063210 China*

** e-mail: zhyn@ncst.edu.cn*

Received February 28, 2022; revised March 21, 2022; accepted March 23, 2022

Abstract—Flower-like $SrTiO_3$ was prepared by hydrothermal method and $BiVO_4$ was prepared by sol–gel method, and then the two materials were fully mixed under the condition of calcination at 500°C for 2 h. The samples were characterized by X-ray diffraction (XRD), scanning electron microscopy (SEM) and UV–Vis diffuse reflectance spectroscopy (DRS) and electrochemical impedance spectroscopy (EIS). The results showed that the $BiVO_4$ nanoparticles were embedded on the flower-like $SrTiO_3$, and the heterojunction between $BiVO_4$ and $SrTiO_3$ was formed which effectively improved the migration efficiency of photogenerated carriers. The UV–Vis test results indicated that the corresponding range of STO–10 wt % BVO composite photocatalyst changes from 380 to 490 nm, and the photocatalytic efficiency reached 72% by degrading tetracycline hydrochloride (TC) under simulated sunlight. Mechanism analysis shows that the type I heterojunction is successfully built between $SrTiO_3$ and $BiVO_4$, which promotes the migration and separation of photogenerated carriers and reduces the recombination rate of photogenerated electrons and holes.

Keywords: flower-like strontium titanate, bismuth vanadate, heterostructure, photocatalysis, tetracycline

DOI: 10.1134/S0036024422130210

INTRODUCTION

The development of new environmentally friendly photocatalytic materials is of great significance to today's society. $SrTiO_3$ is a kind of perovskite photocatalyst, which belongs to cubic crystal system and lattice constant is 3.905 Å [1, 2]. $SrTiO_3$ has attracted the attention of researchers due to its suitable band structure (conduction band position is −1.13 eV, valence band position is 2.14 eV [3]), good thermal and chemical stability, more photocatalytic sites and better photocorrosion resistance [4]. However, pure $SrTiO_3$ has some disadvantages such as easy recombination of photogenerated electron holes and slow photocarrier migration rate, leading to its low photocatalytic activity [5, 6]. In order to further improve the photocatalytic performance of $SrTiO_3$, many researchers have carried out a large number of modification studies on $SrTiO_3$ in recent years. These modification methods can be roughly divided into two categories: One is to modify the morphology of strontium titanate, such as changing the particle size, aggregation state and crystal structure [7] of its nanoparticles. The purpose is to increase the specific surface area of the material and improve the photocatalytic ability of strontium titanate. Zhu [8] synthesized $SrTiO_3$ nanoparticles coated with P123 using the amphiphilic polymer poly(ethylene oxide)-poly(propylene oxide)-poly(ethylene oxide) (PEO-PPO-PEO, P123) as a template. The photocatalytic test results showed that compared with pure $SrTiO_3$ particles, this kind of $SrTiO_3$ particles coated with hydrophilic material can improve the photocatalytic hydrogen production efficiency by 31 times. Secondly, the doping modification of strontium titanate can be doped with metal [9], non-metal [10] or form a heterojunctions [11] with it. Tan et al. [12] prepared W–Ag co-doped $SrTiO_3$ by sol–gel method, and studied the photocatalytic activity and efficiency improvement mechanism of W–Ag co-doped $SrTiO_3$ with methylene blue (MB) as the target pollutant. The results show that under simulated sunlight conditions, the degradation efficiency of W–Ag co-doped $SrTiO_3$ within 6 h is almost 5 times that of pure $SrTiO_3$. According to references [13–16], $BiVO_4$ (conduct band is 0.31 eV, and valence band is 2.78 eV) has a suitable band structure to modify $SrTiO_3$ (conduct band is −1.13 eV, and valence band is 2.14 eV). The construction of $SrTiO_3/BiVO_4$ composite material is expected to improve the band structure of $SrTiO_3$, promote the separation of electrons and holes, and improve the photocatalytic activity. However, there are only a few reports on $SrTiO_3/BiVO_4$ hetero-

junction structures, and generally, only low load rates have been studied. For example [17], the removal of sulfamethoxazole by $SrTiO_3/BiVO_4$ system was studied under visible light. On the other hand, $BiVO_4Ru/SrTiO_3$:Rh composite Z-scheme photocatalyst for solar water splitting.

Therefore, the project team prepared flower-like $SrTiO_3/BiVO_4$ composite photocatalyst by calcination of strontium titanate prepared by hydrothermal method and bismuth vanadate prepared by sol–gel method at 500°C for 2 h. The properties of flower-like $SrTiO_3/BiVO_4$ and the effect of $BiVO_4$ content on the photocatalytic performance of $SrTiO_3$ were studied in detail. The photocatalytic degradation of Tetracycline (TC) hydrochloride in aqueous solution was studied to evaluate the photocatalytic activity of the catalyst. The reaction mechanism of flower-like $SrTiO_3/BiVO_4$ heterojunction was studied by combining electrochemical impedance spectroscopy (EIS).

EXPERIMENTAL

Chemicals

Tetrabutyl titanate ($C_{16}H_{36}O_4Ti$, AR), strontium nitrate ($Sr(NO_3)_2$, AR), ethylene glycol ($(CH_2OH)_2$, AR), sodium hydroxide (NaOH, AR), nitric acid (HNO_3, AR), ammonium hydroxide (NH_4NO_3, AR), bismuth nitrate pentahydrate ($Bi(NO_3)_3{\cdot}5H_2O$, AR), partial ammonium vanadate (NH_4VO_3, AR), monohydrate citric acid ($C_6H_{10}O_8$, AR) were purchased from Shanghai Aladdin Biochemical Technology Co., Ltd. (SABTC, Shanghai, China). Anhydrous ethanol (C_2H_5OH, AR) was purchased from Tianjin Tianli Chemical Reagent Co., Ltd. (TTCRC, Tianjin, China). All reagents were used without any further purification.

Synthesis of $SrTiO_3$

STO is synthesized by hydrothermal method. Briefly, a certain amount of $C_{16}H_{36}O_4Ti$ was dissolved in $(CH_2OH)_2$ for 10 min by stirring, and then 0.5 mol/L Sr $(NO_3)_2$ was added to $C_{16}H_{36}O_4Ti$ solution. After stirring for 1 h, 1mL, 25 mol/L NaOH was added directly to the above solution. Finally, the mixture was transferred to a 100 mL reactor and kept at 180°C for 24 h. The product was then centrifugated and washed with C_2H_5OH and deionized water for 3 times successively. Finally, after holding at 60°C for 20 h, the dried white solid was placed in a mortar and ground into powder to prepare STO powder.

Synthesis of $BiVO_4$

BVO was prepared by sol–gel method. In other words, 2.425 g $Bi(NO_3)_3{\cdot}5H_2O$ was dispersed into the diluted 25 mL 10% HNO_3 solution, stirred with magnetic force for 15–20 min, then 2.104 g $C_6H_{10}O_8$ was added, and violently stirred to obtain a uniform and stable white solution, denoted as solution I. Then 0.5 g NH_4VO_3 was dissolved in 20 mL 90°C distilled water and stirred in a constant temperature water bath at 80°C. After 15 min, 2.1004 g $C_6H_{10}O_8$, which had been weighed, was added and stirred until a uniform and stable dark blue solution was obtained, which was recorded as solution II. Then, liquid II was slowly added into liquid I, and the color of the solution gradually deepened, and finally appeared dark green, which was recorded as solution III. Then the pH of solution III was adjusted to 6.5 with NH_4NO_3. Then, the liquid III was placed in a constant temperature water bath at 80°C and stirred continuously. After dark blue gel was formed, the liquid III was removed and transferred to a drying oven at 70°C for 12 h. Wait until the gel in the beaker forms a "bread" shape and remove. Finally, the dry dark yellow solid was ground into powder in a mortar and calcined at 500°C for 2 h to obtain $BiVO_4$ powder [18].

Fabrication of Flower-Like $SrTiO_3/BiVO_4$ Heterostructures

Flower-like $SrTiO_3/BiVO_4$ heterojunction was constructed by calcination of STO and BVO materials in muffle furnace at high temperature. 0.05, 0.15, and 0.25 g $BiVO_4$ were accurately weighed and added into 3 parts of 30 mL deionized water for stirring for 30 min. Then the ultrasonic vibration was continued for 15 min in three times, 5 min each time. 0.5 g $SrTiO_3$ was added to stir for another 30 min, and then the ultrasonic vibration was divided into three times for 15 min. The flower-like $SrTiO_3/BiVO_4$ composite powder was prepared by steam drying in a 60°C water bath and calcination for 2 h at 500°C. The mass percentage of $BiVO_4$ in the sample was 10, 30, and 50 wt % [19]. The samples were termed as STO–*X*, wt % BVO (*X* = 10, 30, and 50 are the mass contents of BVO with respect to the STO mass).

Characterizations

The instrument used for qualitative phase analysis and testing is the X-ray powder diffraction (XRD) instrument manufactured by The Japanese Neo-science Corporation, the model is D/MAX2500PC (Cu target, K_α rays). In order to more intuitively and clearly observe the microscopic appearance of the sample, S-4800 field emission electron microscope manufactured by Hitachi Corporation of Japan was adopted in this experiment. The optical properties of the samples were characterized by UV–Vis DRS tests, which use UV-9000S UV–Vis spectrophotometer produced by Shanghai Yuanyan Instrument Co., Ltd. In order to analyze the samples by electrochemical impedance spectroscopy (EIS), the CHI660D elec-

trochemical workstation of Shanghai Chenhua Instruments was used for characterization.

Photocatalytic Testing

Tetracycline hydrochloride is light yellow powder, soluble in water, colorless solution by the naked eye cannot distinguish between solubility of change, and the adjustment of solubility is proportional to the absorbance changes [20, 21], therefore, can be measured by its absorbance to embody its solubility change so as to calculate the rate of catalyst for the degradation of tetracycline hydrochloride, and in this way can determine the degradation effect of catalysts and degradation ability.

Tetracycline hydrochloride solution with an initial concentration of 50 mg/L was first prepared, and then 20 mL tetracycline hydrochloride solution was measured and added to the photocatalytic reactor. Then 50 mg $SrTiO_3/BiVO_4$ composite material was added, and stirred for 30 min under the condition of dark. Gets tetracycline molecules on the surface of catalyst adsorption stripping balance, and then open the light emitting diode (LED) for photocatalytic reaction, every 30 min take a sample (the response time of 150 min), centrifugal after take supernatant fluid and the light of 365 nm absorbance measurement, and according to the changes of the measured absorbance to judge the degradation degree of the tetracycline hydrochloride. The optimum compound ratio of tetracycline hydrochloride was studied by contrast experiment.

RESULTS AND DISCUSSION

Chemical Composition (XRD)

In order to investigate the crystal structure of the prepared samples, the materials were characterized by X-ray diffractometer. It can be seen from Fig. 1 that the diffraction peaks of $SrTiO_3$ appear at 32.4°, 46.5°, and 57.8°. These peaks correspond to the perovskite phase $SrTiO_3$ (PDF no. 35-0734) (110), (200), (211) crystal planes, indicating that $SrTiO_3$ still maintains the original crystal phase after calcination, and there are no other impurities. Compared with $SrTiO_3$, the new characteristic peaks of the composite were all assigned to $BiVO_4$ (PDF no. 14-0688), indicating that the addition of $BiVO_4$ did not change the phase structure of $SrTiO_3$. The two are independent of each other, but tightly combined, which is favorable for them to directly form a heterojunction.

Morphology Characterization (SEM)

The microscopic morphologies of the as-prepared samples were investigated by scanning electron microscopy, as shown in Figs. 2a–2d. It is obvious that $SrTiO_3$ particles exhibit petal shape. $BiVO_4$ particles

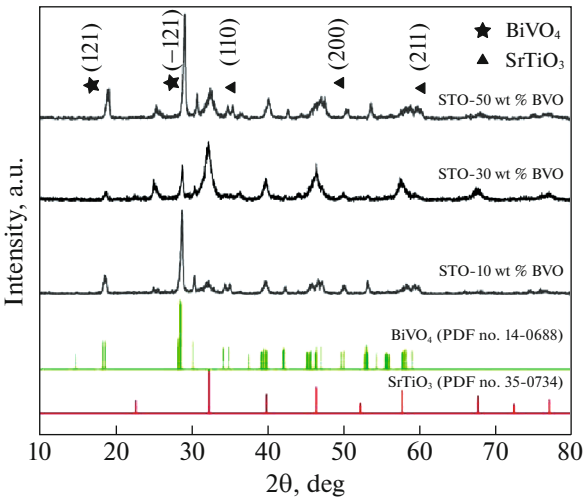

Fig. 1. XRD patterns of as-prepared samples.

are mainly irregularly shaped nanoparticles. After the composite of $BiVO_4$ and $SrTiO_3$, irregular $BiVO_4$ nanoparticles were embedded on the $SrTiO_3$ petals, as shown in Figs. 2c, 2d. The results showed that the $SrTiO_3/BiVO_4$ composite photocatalytic material was successfully prepared. The formed fluffy structure is beneficial to the absorption and utilization of light by the photocatalytic material, and at the same time, the contact area between the photocatalytic material and the pollutant can be increased, and the photocatalytic efficiency can be improved. However, when the content of $BiVO_4$ is too large, $BiVO_4$ particles will agglomerate on the surface of $SrTiO_3$, which will affect the photocatalytic effect.

Optical Properties (UV–Vis DRS)

In order to characterize the light absorption properties of the $SrTiO_3/BiVO_4$ composite photocatalyst, the samples were subjected to UV–Vis DRS test, as shown in Fig. 3. We can find that the absorption edge of $SrTiO_3$ is around 380 nm, indicating that $SrTiO_3$ only absorbs ultraviolet light, which is determined by the inherent band gap of $SrTiO_3$; the absorption edge of $BiVO_4$ is around 460 nm, indicating that $BiVO_4$ can absorb visible light, which is also determined by its narrow band gap. Comparing three kinds of $SrTiO_3/BiVO_4$ composite photocatalysts with different composite contents, only the absorption edge of STO-10 wt % BVO composite photocatalyst is obviously red-shifted, and its photoresponse range is expanded to about 490 nm. This indicates that by recombining with an appropriate amount of $BiVO_4$, the band gap width of $SrTiO_3$ is reduced, and the photoresponse range of $SrTiO_3$ to visible light is enlarged at the same time.

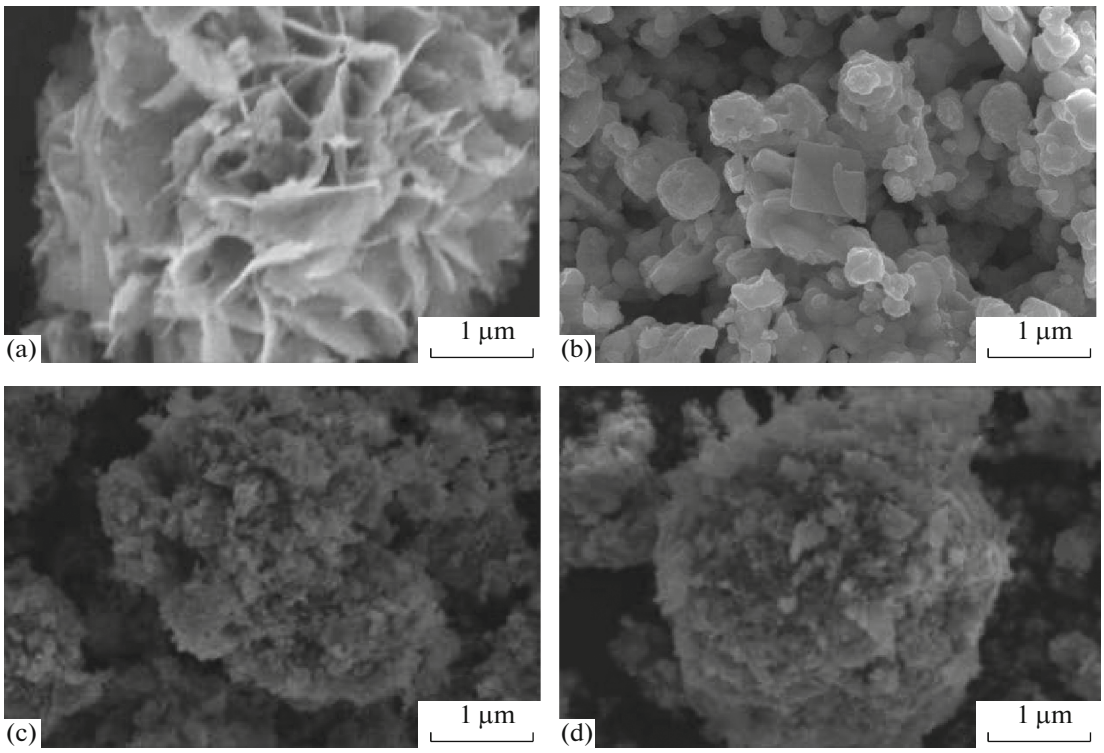

Fig. 2. SEM images of $SrTiO_3$ (a), $BiVO_4$ (b), STO-10 wt % BVO (c), and STO-50 wt % BVO (d).

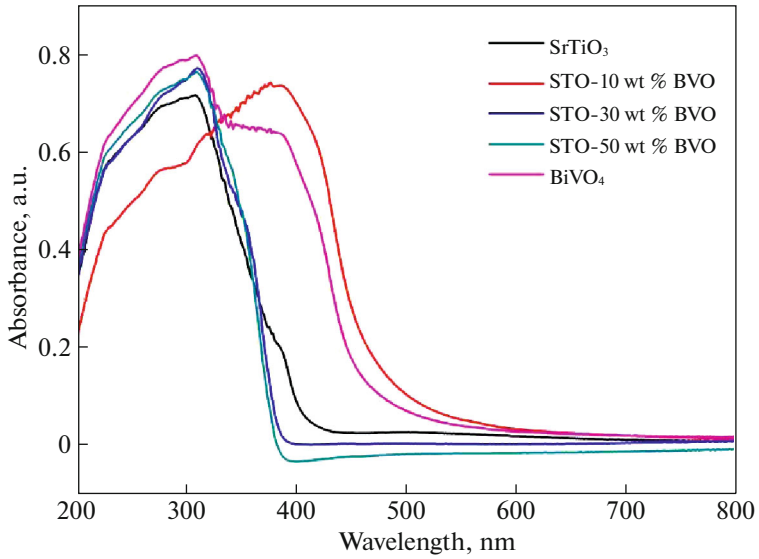

Fig. 3. UV–Vis diffuse reflectance spectra of as-prepared samples.

Electrochemical Impedance Spectroscopy Analysis (EIS)

In order to study the separation of photogenerated electrons and holes, electrochemical impedance tests were performed. As can be seen from Fig. 4, except for the STO-50 wt % BVO composite photocatalyst, the impedance arc radius of the other two composite photocatalysts is smaller than that of pure $SrTiO_3$. STO-10 wt % BVO and STO-30 wt % BVO have the smallest resistance arc radius, and there is little difference between them. This indicates that the composite photocatalysts, especially STO-10 wt % BVO and STO-30 wt % BVO, enhance the separation and transfer speed of photogenerated charges. This can be consid-

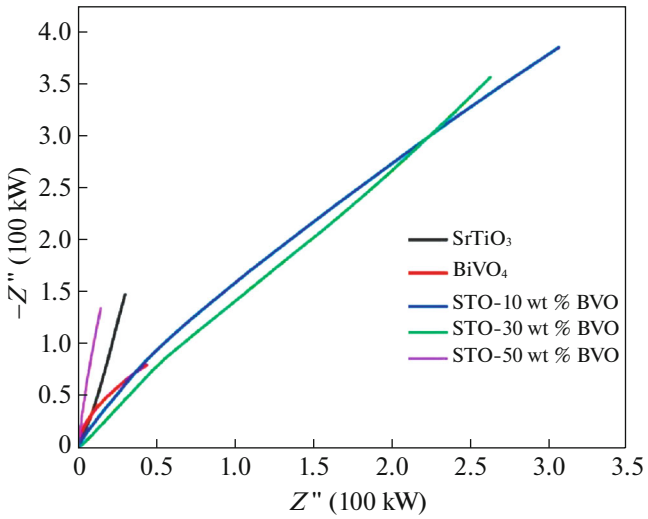

Fig. 4. Electrochemical impedance plots of as-prepared samples.

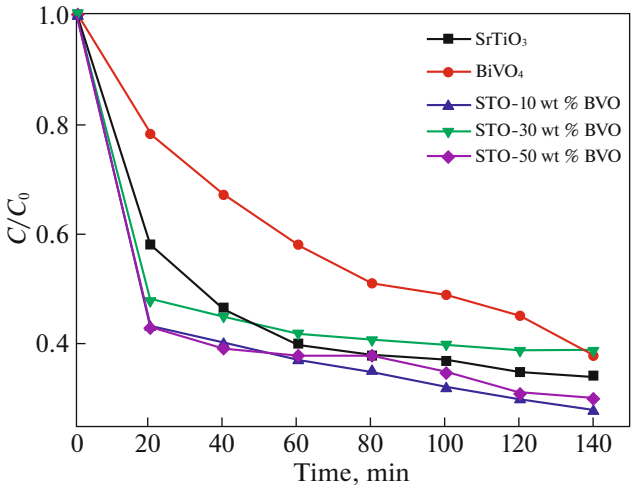

Fig. 5. Graph of the TC degradation efficiency of as-prepared samples under visible light.

ered as the formation of a heterojunction structure when $BiVO_4$ and $SrTiO_3$ are recombined. The heterojunction promotes the separation and transfer of photogenerated electrons and holes, and also inhibits the recombination of photogenerated charges.

Photocatalytic Activity

In order to further explore the photocatalytic performance of the prepared $SrTiO_3/BiVO_4$ composite photocatalyst, TC was degraded under visible light irradiation to characterize its photocatalytic activity. The results are shown in Fig. 5. In the whole degradation experiment, the TC degradation efficiency of pure $SrTiO_3$ reached 66% after 140 min, while pure $BiVO_4$ reached 62% after 140 min. The TC degradation efficiency of STO-10 wt % BVO reaches 72%, STO-30 wt % BVO reaches 61%, and STO-50 wt % BVO reaches 70%. It can be seen from Figs. 2c, 2d that when the amount of $BiVO_4$ is too much, $BiVO_4$ particles agglomerate and cover the surface of $SrTiO_3$, reducing the light contact area of $SrTiO_3$, resulting in a decrease in the photodegradation efficiency of $SrTiO_3$. So the degradation efficiency of STO-50 wt % BVO is lower than that of STO-10 wt % BVO. The photocatalytic performance of $BiVO_4$ is not as good as that of $SrTiO_3$, so the degradation efficiency of STO-30 wt % BVO is lower than that of STO-10 wt % BVO. But with the increase of $BiVO_4$ content, $BiVO_4$ became the main catalyst for degradation. This is also reflected in the fact that the degradation efficiency of the STO-50 wt % BVO is higher than that of the STO-30 wt % BVO. The above results show that the efficiency of $SrTiO_3$ degradation of TC under visible light can be improved by compounding an appropriate amount of $BiVO_4$.

Reaction Mechanism

Based on the above experimental results, explore the possible mechanism of $SrTiO_3/BiVO_4$ heterojunction degradation of TC (Fig. 5). From Fig. 6, we can know that the composite photocatalyst forms a type I heterojunction. That is, the electrons in $SrTiO_3$ valence band immediately migrated from the conduction band of $SrTiO_3$ to the conduction band of $BiVO_4$ after being stimulated by light. At the same time, the holes left by electron transition in $SrTiO_3$ valence band will migrate to $BiVO_4$ valence band so as to promote the separation of $SrTiO_3$ photoelectron–hole pair. Then, oxidation and reduction reactions occur on $BiVO_3$. It can be seen that the formation of a heterojunction between $SrTiO_3$ and $BiVO_4$ can increase the separation efficiency of photogenerated electron-hole pairs, thereby increasing the photocatalytic activity of the composite photocatalyst for degradation of TC.

However, in the experimental system, $BiVO_4$ is also a photocatalyst, which can absorb light and produce valence band electron transition. As the photogenerated electrons migrated from $SrTiO_3$ will accumulate in the conduction band of $BiVO_4$, and the holes will also accumulate in the valence band of $BiVO_4$. These two phenomena greatly reduce the separation rate of $BiVO_4$ photocarrier, and $BiVO_4$ is more of a “sacrificial agent [22]” in this system. Later work center of gravity can be placed in the two substances build depth analysis of the mechanism of the heterojunction direction, such as how to improve the band structure of these two materials to build better heterojunction

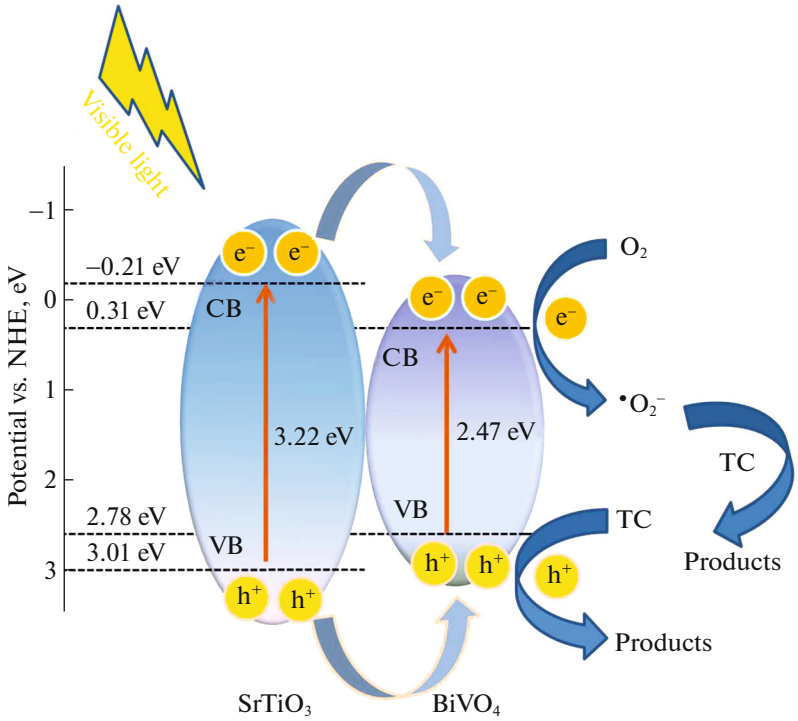

Fig. 6. Schematic diagram of heterojunction level and interfacial charge transfer in $SrTiO_3/BiVO_4$ composite photocatalytic.

Z type [23]. For example, in [3] sample under investigation exhibits photocatalytic performance 91% within 60 min towards sulfamethoxazole degradation.

CONCLUSIONS

Flower-like $SrTiO_3/BiVO_4$ composite photocatalysts were prepared by mixed calcination at 500°C for 2 h. XRD and SEM results showed that $BiVO_4$ nanoparticles were embedded on flower-like $SrTiO_3$, and the heterojunction structure was formed between $SrTiO_3$ and $BiVO_4$. The light response range of STO-10 wt % BVO composites extended to 490 nm by UV–Vis DRS testing analysis. The degradation efficiency of the STO-10 wt % BVO composite reached 72% by photodegrading tetracycline hydrochloride solution under visible light irradiation. Through the analysis of the photocatalytic mechanism of the composite photocatalyst, it is mainly due to the structure of the type I heterojunction and the suitable specific surface area of the sample.

ACKNOWLEDGMENTS

This work was financially supported by the Hebei Province Natural Science Foundation of Iron and Steel Joint Fund of China (grant no. E2021209002); project of Tangshan Science and Technology Bureau (no. 21130211D); and preparation of strontium titanate/graphitic carbon nitride composites and their photocatalytic mechanism (X2021158).

CONFLICT OF INTEREST

The authors declare that they have no conflicts of interest.

REFERENCES

1. M. A. Ferreira, G. T. S. T. da Silva, and O. F. Lopes, Mater. Sci. Semicond. Process. **108**, 104887 (2020).
2. B. L. Phoon, C. W. Lai, and J. C. Juan, Int. J. Energy Res. **43**, 5151 (2019).
3. J. Li, F. Wang, and L. Meng, J. Colloid Interface Sci. **485**, 116 (2017).
4. H. W. Kang, S. N. Lim, and S. B. Park, Int. J. Hydrogen Energy **37**, 5540 (2012).
5. X. L. Jing, Y. L. Shao, and Y. Zheng, Mol. Catal. **34**, 559 (2020).
6. G. Z. Wang, H. Chen, and X. K. Luo, Int. J. Quantum Chem. **117**, 25424 (2017).
7. J. J. Shan, PhM Thesis (Univ. G. F. Wang, 2018).
8. L. Y. Zhu, PhD Thesis (Univ. Lu YL, Fu ZP, 2020).
9. S. Ouyang, H. Tong, and N. Umezawa, J. Am. Chem. Soc. **134**, 1974 (2012).
10. Z. Fei, J. Chem. Commun. **48**, 8514 (2012).
11. H. Kato, Y. Sasaki, and N. Shirakura, J. Mater. Chem. A **1**, 12327 (2013).
12. C. Tan, D. Y. Zuo, and J. S. Li, J. Environ. Chem. **40**, 3217 (2021).
13. Z. B. Jiao, T. Chen, and J. Y. Xiong, Sci. Rep. **3**, 2720 (2013).
14. Z. B. Jiao, T. Chen, and H. C. Yu, J. Colloid Interface Sci. **419**, 95 (2014).

15. Y. Kim, K. Choi, and J. Y. Jung, J. Environ. Int. **33**, 370 (2007).
16. J. H. Li, W. Zhao, and Y. Guo, J. Appl. Surf. Sci. **351**, 270 (2015).
17. Q. X. Jia, A. Iwase, and A. Kudo, J. Chem. Sci. **5**, 1513 (2014).
18. H. Xu, C. Wu, and H. Li, J. Appl. Surf. Sci. **256**, 597 (2009).
19. Q. Z. Wan, S. L. Zhang, and D. H. Jiao, CN Patent CN201610943494.6 (2019).
20. J. M. Song, W. R. Zhu, and X. L. Wang, J. Anhui Univ. (Nat. Sci.) **45**, 72 (2021).
21. Z. R. Zhu, H. W. Xia, and H. Li, J. Dalian Polytech. Univ. **40** (06), 421–426 (2021).
22. W. C. Lin, J. Jayakumar, and C. L. Chang, J. Appl. Catal. B **298**, 120577 (2021).
23. Y. Yuan, R. T. Guo, and L. F. Hong, J. Mater. Today Energy **21**, 100829 (2021).